High-Dimensional Characterization of Tertiary Lymphoid Structures Using Orion™, HALO®, and HALO AI

Ghislaine Lioux[2], Edward Lo[1], Tad George[1]
[1]RareCyte, Inc., Seattle, WA [2]Indica Labs, Albuquerque, NM

Abstract:

Background. Inflammatory tumor microenvironments contain diverse immune and stromal cell populations whose composition and spatial organization influence immune activation and clinical response to immunotherapy. Tertiary lymphoid structures (TLS), composed of organized B and T cell aggregates, represent sites of local immune regulation across cancer, autoimmunity, and lymphoid organs. Here, we present an integrated workflow combining high-resolution, whole-slide multiplexed immunofluorescence imaging with AI-powered image analysis to define immune phenotypes based on multiplex markers on three human tissues with prominent lymphoid aggregates: tonsil (physiological TLS), salivary gland (autoimmune TLS in Sjogren's syndrome), and non-small cell lung cancer (tumor-associated TLS).

Methods. Slides were imaged using the Orion™ Instrument (RareCyte) and analyzed using HALO® and HALO AI (Indica Labs). HALO AI classifiers were trained to segment tissue compartments (epithelium, stroma, B- and T-cell zones) across the three tissues. The Highplex FL module was used for consistent HALO® and HALO AI-driven cell segmentation and supervised phenotyping based on biomarker intensity and cell compartment localization. The HALO® High Dimensional Analysis module was used to perform unsupervised phenotyping on cell object data generated by the Highplex FL module. Clustering was conducted with K-means and Phenograph, and results were visualized with UMAP, enabling the discovery of phenotypic diversity within TLS beyond predefined gating strategies.

Results. Tissue segmentation and cellular phenotyping accurately delineated TLS architecture in all three tissues. Comparison of TLS across tissue types revealed distinct patterns of immune cell composition, spatial organization and activation states. Salivary glands showed periductal TLS enriched in CD4+ T cells and M1 Macrophages, while NSCLC TLS displayed variable maturation with increased checkpoint expression and stromal remodeling. Unsupervised clustering using Phenograph conducted in the NSCLC to compare TLS in the Immune-Rich Tumor zone and Dense Tumor zone also identified further differences to the ones captured by supervised gating, highlighting the power of combining prospective phenotyping and data-driven analysis.

Conclusions. This Orion–HALO–HALO AI workflow enables high-dimensional, spatially resolved characterization of TLS and immune microenvironments across physiologic, autoimmune, and tumor contexts. The combination of AI-based segmentation, supervised phenotyping, and unsupervised clustering provides a scalable, flexible approach for translational and clinical research applications in immuno-oncology and tissue immunopathology.

Orion multiplexing imaging

Preparation

Standard microscope slide and tissue section

FFPE and fresh frozen samples + AF quench

Staining

Single-round staining, standard IHC/IF protocols

OPTIONAL: bank for up to 1 year

Image acquisition

20 channels, whole slide, one scan

OPTIONAL: remove coverslip and perform H&E staining and scanning

18 plex
Hoechst
CD45
Ki67
CD3
CD20
CD4
CD163
CD8a
E-cadherin
PD-L1
PD-1
CD45RO
FOXP3
CD68
CD31
SMA
Pan-CK
Vimentin

Orion OME.tiff

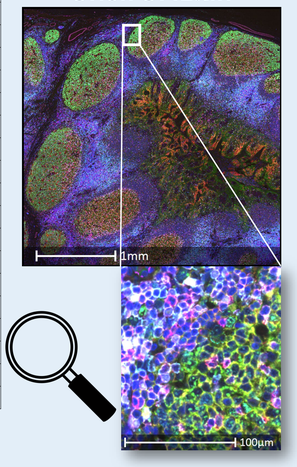

HALO® image analysis

AI tissue classification

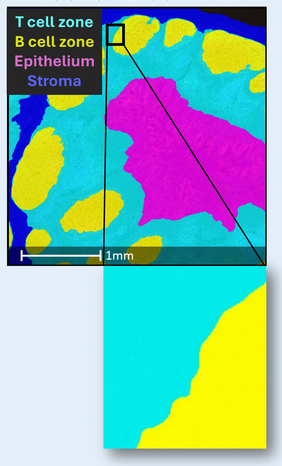

Cell segmentation & phenotyping

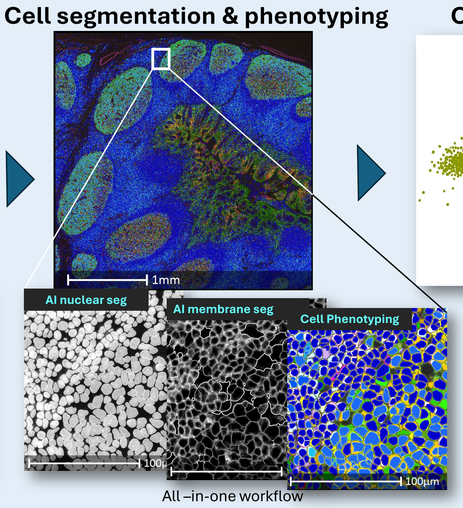

Clustering & UMAP

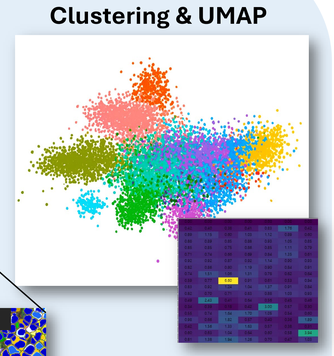

All –in-one workflow

Figure 1. Imaging and image analysis workflow steps. FFPE slide sections of human tonsil, salivary gland, and NSCLC tissues were stained with the complete 18-plex panel and imaged on the Orion instrument in a single scan. The 18-plex IF panel targets markers of leukocytes (CD45), B cells (CD20), T cells (CD3, CD4, CD8), regulatory T cells (FOXP3), macrophages (CD68, CD163), checkpoint molecules (PD-1, PD-L1), memory/activation (CD45RO), endothelium (CD31), proliferation (Ki-67), and epithelial cells (cytokeratin, E-cadherin), along with Hoechst. The HALO® software allows AI-driven tissue segmentation of T-cell zones / B-cell zones and consistent cell segmentation across the three tissue types. Cells were segmented and phenotyped using the HALO® Highplex FL module and unsupervised clustering was used to identify functional cell groups in an unbiased fashion.

Molecular comparison of TLS in three tissues

	Tonsil (reactive)	Salivary gland (Sjogren's syndrome)	Lung (NSCLC)
Whole slide IF images. The **tonsil** contains B cell follicles (yellow) surrounded by T cell zones (magenta). In **salivary gland**, periductal TLS with B cell and T cell zones form near intact ductal epithelium (green). In **NSCLC**, tumor-associated TLS appear in the stroma, adjacent to or infiltrating epithelial tumor nests (green).	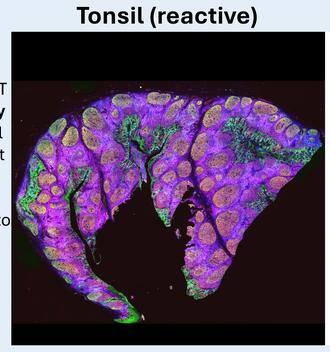	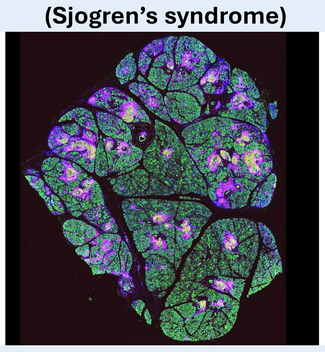	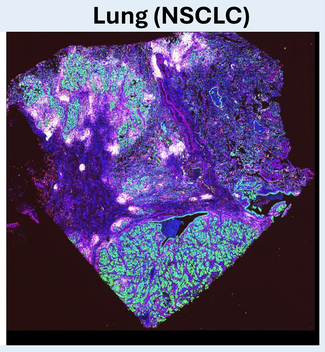
Lymphoid architecture. In the **tonsil**, B cell follicles are depicted in green, Macrophages (red) are distributed throughout the tissue. In the **salivary gland**, B and T cell organization resembles that of tonsils, except for a periductal arrangement. In **NSCLC**, TLS share a B cell core and a T cell surrounding but with more irregular organization.	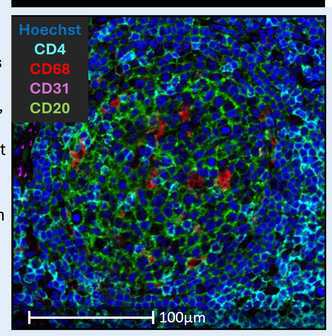	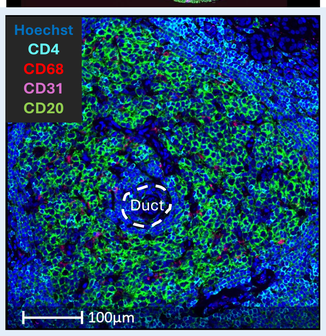	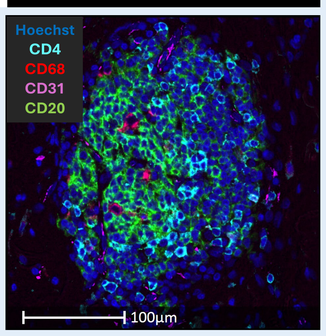
Proliferation & immune response. In the **tonsil**, PD-1+ cells cluster within germinal centers alongside abundant Ki-67+ proliferating cells. In the **salivary gland**, PD-1+ and Ki-67+ periductal concentrations reflect autoimmune activation. In **NSCLC**, cells are more dispersed.	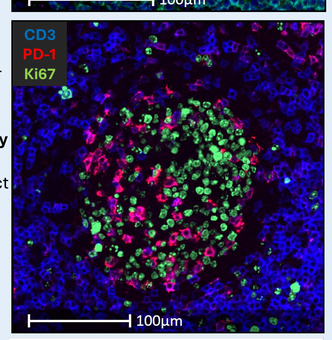	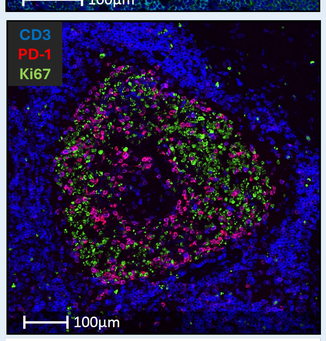	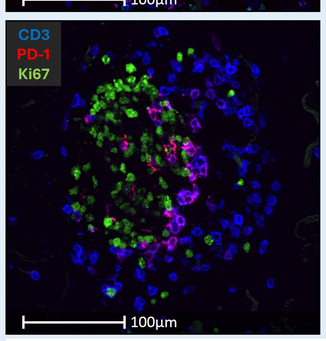
Cell composition Treemap comparison of TLS. K-means (k=7) highlights main tissue differences. **Tonsil** validates K-means labels with abundant B-cell zones and follicular T cells dynamics. In the **salivary gland** prevalence of CD4 T cells and presence of M1 macrophages reflect autoimmune inflammation. **NSCLC** are T cell–heavy, vessel-associated, and partially immunosuppressive.	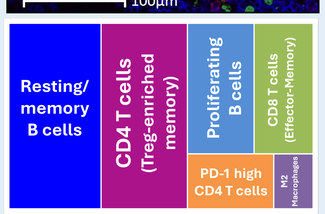	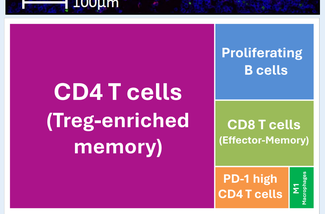	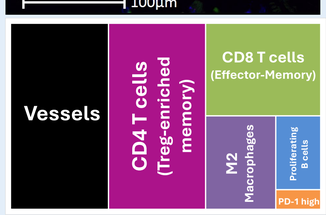

Proliferating B cells · Resting/memory B cells · Effector-memory CD8 T cells · M1-like macrophages · M2-like macrophages · PD-1 high CD4 T cells · CD4 T cells (Treg-enriched memory) · Vessels

Figure 2. Comparative cellular composition of tertiary lymphoid structures across tonsil, salivary gland (Sjogren's), and NSCLC. Here Tonsil tissue appears fully mature with robust B-cell germinal centers (GC) associated with follicular T helper cells. In Sjogren' s syndrome TLS are T-cell heavy, with functional but imbalanced B cell GCs. In cancer, TLS may promote anti-tumor responses, but are simultaneously restrained by suppressive networks, which may determine whether they are prognostically beneficial.

NSCLC: Characterization of TLS in the Dense Tumor zone vs Immune Rich zone

Lung (NSCLC): Immune-Rich vs Dense Tumor

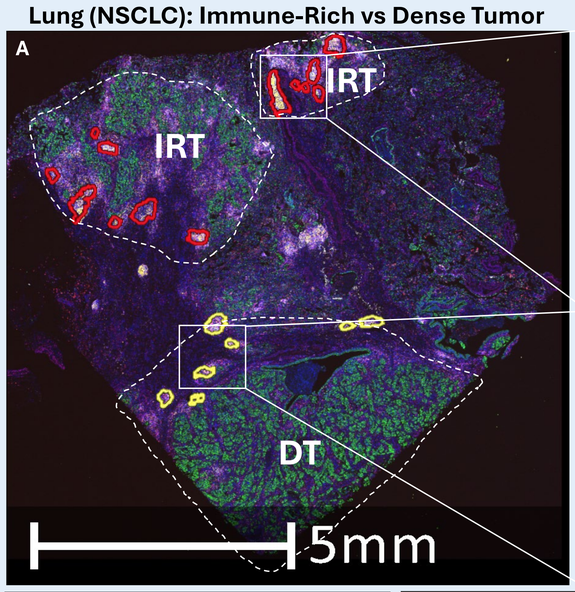

Density Heatmap prolif. B cells

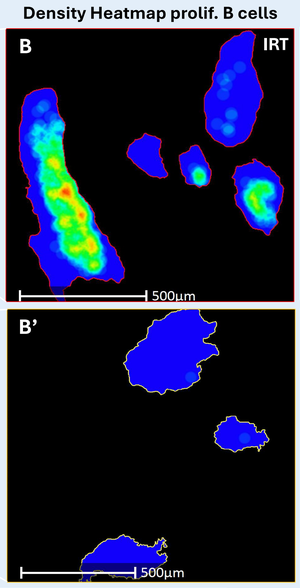

Spatial Map

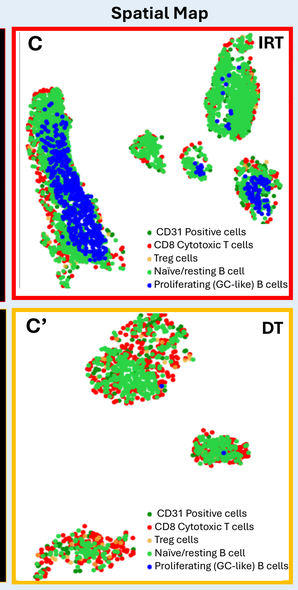

D Phenograph Feature Heatmap IRT

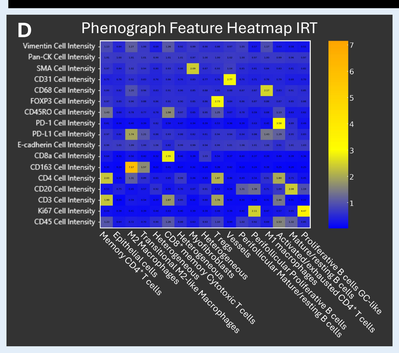

D' Phenograph Feature Heatmap DT

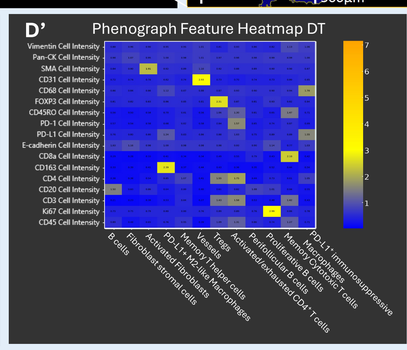

E

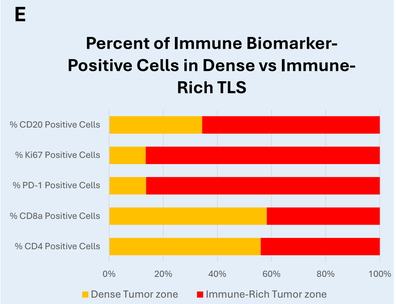

F TLS Phenograph cluster proportions

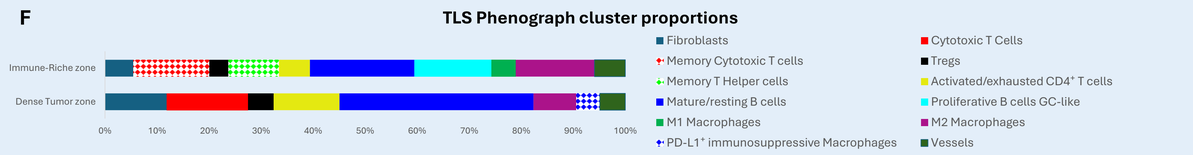

Figure 3. Comparative cellular architecture of Immune-Rich vs Dense Tumor zones in NSCLC. Immune-Rich tumor (IRT) and Dense Tumor (DT) zones were identified and separated for cell analysis and biomarker evaluation in HALO® (A, E). The DT zone shows depleted proliferative B cells and fewer B cells overall compared to the IRT. This quantification was confirmed with spatial analysis in HALO® (B, B', C, C'). Density heatmaps (B) and spatial plots (C) of the IRT display higher densities of proliferating GC-like B cells than the DT (B', C'). To complement the previous prospective cell phenotyping using standard gating analysis, unsupervised Phenograph clustering was performed in HALO®. The Phenograph algorithm was applied to compare the TLS of the IRT (D) and DT cell populations (D'). The identified cell populations were then quantified and visualized as percentages in bar plots (F).
The IRT shows high numbers of mature B cells along with proliferative GC-like B cells like the tonsil (F, Fig. 2). The presence of memory cytotoxic T cells and memory helper T cells in the IRT indicates active immune surveillance. TLS in the IRT, unlike those in the DT, also contain some M1 macrophages, which are pro-inflammatory and tumor-suppressive. In contrast, TLS in the DT are shaped by stromal fibroblasts and immunosuppressive M2 and PD-L1+ macrophages. Furthermore, in the DT, cytotoxic T cells (CTLs) are present but skewed toward fewer memory CTLs and more exhausted CD4+ T cells.

Conclusion:

By integrating Orion high-plex imaging with HALO and HALO AI, we achieved scalable, spatially resolved phenotyping showing that TLS location and tissue context shape their cellular composition and functional potential across physiologic, autoimmune, and tumor settings. This workflow was also used within different zones of the same tissue to explain heterogeneous immune control across a single tumor. Here we showed that In NSCLC, immune-rich TLS support germinal center B-cell maturation and cytotoxic T-cell activity, whereas dense tumor zone TLS are fibroblast- and macrophage-dominated, restricting lymphocyte function and driving intra-tumoral heterogeneity. This workflow provides a powerful framework for translational research and spatially targeted therapies (e.g., stroma/TAM modulation in dense zones vs checkpoint modulation in immune-rich zones).